6

CLASSIFICATION OF EARTH TERRAIN USING POLARIMETRIC SYNTHETIC APERTURE RADAR IMAGES

J. A. Kong, S. H. Yueh, H. H. Lim,
R. T. Shin, and J. J. van Zyl

6.1 Introduction

Classification of earth terrain within an image is one of the many important applications of polarimetric data. A systematic classification procedure will place the classification process on a more quantitative level and reduce the amount of photo-interpretation necessary [*Evans*, 1986]. Single feature and multifrequency classifications have been used in the past, but classification can now be applied to fully polarimetric data which have become available due to recent developments in radar technology. It has been shown that Bayes classification using

fully polarimetric data yields optimal results as compared to classification performance using any subset of the complete polarimetry [*Kong et al.*, 1988; *Lim et al.*, 1989].

In some cases, the absolute magnitude and phase of the radar returns are not reliable features for data classification purposes. This is due to the fact that radar system calibration procedures vary in accuracy as well as the fact that they cannot account for attenuation and phase shifts caused by atmospheric distortions. Normalization schemes [*Yueh et al.*, 1988], which preserve only the relative components of the returns, were applied to radar polarimetry in order to circumvent this problem. Previously, normalized polarimetric classification schemes were implemented by assuming a multivariate Gaussian distribution for normalized data [*Kriegler et al.*, 1971; *Smedes et al.*, 1971]. However, this technique yields inconsistent results since the probability of error, as well as classification performance, becomes a function of the particular normalization scheme selected. Therefore, the optimal normalized classification algorithm will be employed in which the probability density function (PDF) is derived under the same assumption used to derive the PDF for the unnormalized fully polarimetric data. When employing this normalization process, the classification result and the probability of error will be independent of the normalization function [*Yueh et al.*, 1988].

From an alternate point of view, unsupervised classification may also be applied. The polarization state of the received wave may be compared to that of the transmitted wave in order to deduce the properties of the scatterer. This algorithm classifies terrain elements based on the relationship between the orientation angle and handedness of the transmitting and receiving polarization states. Classification is then based solely on the properties of the scatterer and not on any *a priori* training data [*van Zyl*, 1987].

In section 2 of this chapter, both the supervised and unsupervised classification techniques are applied to San Francisco Bay and Traverse City Synthetic Aperture Radar (SAR) images, supplied by the Jet Propulsion Laboratory. These images were collected at L-band (1.225 GHz) with near range along the upper part of the image. There are 896 pixels in the range and 4096 pixels in the azimuth with approximately 10 m by 3 m resolution per pixel. For supervised classification processing, the Bayes technique is used to classify fully polarimetric and normalized polarimetric SAR data. Simpler polarimetric discrimi-

nates, such as the absolute and normalized magnitude response of the individual receiver channel returns, in addition to the phase difference between the receiver channels, are also considered. An unsupervised technique, based on comparing general properties of the Stokes parameters of the scattered wave to that of simple scattering models, is also discussed [*van Zyl,* 1987]. It is shown that supervised classification yields the best overall performance when accurate classifier training data are used, whereas unsupervised classification is applicable when training data are not available.

Besides classifying earth terrain into different classes, there is also considerable interest in determining the optimal polarizations that maximize contrast between two scattering classes in polarimetric radar images [*Swartz et al.,* 1988]. Contrast enhancement is a processing technique which modifies the input data structure so that either the human observer, computer, or other hardware devices can extract certain information from the processed data more readily after the change [*Huang,* 1969]. In the second part of this chapter, the polarimetric properties of the radar returns are utilized to enhance the contrast between two scattering classes. It is assumed that complete *a priori* statistical knowledge of the two scattering classes or types exists and the polarimetric signals backscattered from the two scattering classes are independent. The processing requirement is then to determine the optimal transmitting and receiving polarization state which will maximize the separation of the average power returns between the two classes. Applying such a technique to radar imagery will allow for better discrimination of the two classes.

For two deterministic scatterers, completely characterized by 2×2 complex scattering matrices, *Kozlov* [1979] introduced a method for computing the optimal polarization state which involves transformation of the scattering matrix of each of the two objects into a preferred polarization basis. Solutions involving scattering matrix *co–pol* and *cross–pol* (polarization) *nulls* have also been presented [*Mieras,* 1983; *Nespor et al.,* 1984; *McCormick and Hendry,* 1985]. More recently, *Kostinski and Boerner* [1987] determined the transmitting and receiving polarization state which produced maximum contrast between two classes represented by their Graves power matrices. This technique involved maximizing the expected power return from one deterministic scattering class with respect to another.

Although these are viable procedures when dealing with deter-

ministic scattering classes, they cannot be utilized in the case of statistically distributed scattering objects, e.g., terrain clutter. A deterministic scatterer can be characterized by a scattering matrix, whereas nondeterministic scatterers must be represented either by an average Mueller matrix or, equivalently, by a polarimetric covariance matrix, which are the second order statistics of the scattering matrix. To enhance the contrast between nondeterministic scatterers, the ratio of the average power returns from the two scattering classes must be maximized.

In the case of distributed scatterers in the clear, observability is limited only by background noise. Since the noise in the receiver channels is statistically independent and usually normalized at the same average power, the background noise is generally unpolarized. This implies that when the target-to-clutter ratio is maximized, under the assumption that the distributed scatterer represents the target, whereas background noise denotes clutter, it will be found that the background noise contribution has essentially a constant expected power level [*Giuli,* 1985]. Thus, for targets which are assumed to be in the clear, or independent of a clutter background, maximizing this ratio is equivalent to maximizing the target return power only. Target detection improvement which can be attained by such a procedure has been analyzed by resorting to a Gaussian target model [*Giuli,* 1982] derived from Huynen's target decomposition theorem [*Huynen,* 1978]. Moreover, *van Zyl et al.* [1987] have determined the optimal copolarization state for maximum power return from an isolated, distributed scatterer, represented by its average Mueller matrix.

For the case of two scattering classes, both of which were either fully or partially polarized, *Ioannidis and Hammers* [1979] employed a Lagrange multiplier method to determine the transmitting and receiving polarization state that maximized a target's return in the presence of clutter. The target-to-clutter ratio, expressed in terms of average Mueller matrices, was maximized in order to determine the optimal transmitting and receiving antenna Stokes polarization vectors. *Zebker et al.* [1987] have introduced the polarization signature as a means of displaying polarimetric characteristics of various scatterers. They [*Zebker et al.,* 1987] numerically determined the polarization state which maximized contrast between two classes when the receiving polarization was fixed with respect to that of the transmitter, e.g., co- or cross-polarized returns.

It should be noted that all of the techniques previously discussed for polarimetric enhancement of a target's return in the presence of clutter have maximized the target-to-clutter ratio. However, maximization of the contrast between two classes is not necessarily the same as maximizing the target-to-clutter ratio. For example, the object scattering the most power generally is denoted to signify the target class, whereas the other scattering class is referred to as clutter, although this may not always be the case. If a target in severe clutter is considered, the clutter class may actually scatter more power than the target for some transmitting and receiving polarization states. Moreover, the classes can exhibit different polarimetric correlation coefficients between the receiver channels while having comparable radar cross sections. Thus, the notion of a target and clutter class, in some instances, is not well defined. Note also that, in general, maximization of the target-to-clutter ratio does not provide the same contrast between classes as maximization of the clutter-to-target ratio. Therefore, the problem addressed here is to select the larger of these two values and determine its corresponding polarization state. For this reason, the term contrast ratio will be adopted as opposed to using either the target-to-clutter or clutter-to-target ratios.

Consequently, the procedure implemented in section 3 will determine the transmitting and receiving polarization state which produces maximum contrast, or separation in the average intensity, between the two scattering classes. To realize this objective, the contrast ratio will be maximized, i.e., the *maximum contrast ratio* is computed in order to obtain the optimal linear weighting vector or optimal polarimetric matched filter [*Cadzow,* 1980; *Swartz,* 1988]. Processing polarimetric synthetic aperture radar (SAR) images with this filter performs a polarization synthesis on the data which yields maximum contrast between classes.

6.2 Supervised and Unsupervised Classifications

Supervised and unsupervised classification procedures are developed and applied to SAR polarimetric images in order to identify their various earth terrain components. First, the supervised Bayes classification is presented in section 6.2a where the Bayes Classifier is briefly reviewed. Then the polarimetric Bayes classification procedure is discussed where the distance measures for both unnormalized and nor-

malized data will be used to classify the SAR images into different terrain types. Covariance matrices are computed for each terrain class from selected portions within the image where ground truth is available, under the assumption that the polarimetric data have a multivariate Gaussian distribution. These matrices are then used to train the optimal classifier, which in turn is used to classify the entire image. Simple feature classification, which includes magnitude responses $|HH|$, $|HV|$, and $|VV|$, normalized magnitude responses $|HV|/|HH|$ and $|VV|/|HH|$, and phase differences between channels $\phi_{hh} - \phi_{vv}$, $\phi_{hv} - \phi_{vv}$, and $\phi_{hh} - \phi_{hv}$, will also be discussed. The unsupervised classification procedure, which is based on comparing the general properties of the Stokes parameters to those of some simple scattering models, will be described in section 6.2b where it will be applied to the same images analyzed in section 6.2a.

In addition to the classification based on the high resolution data, four-look classification is performed. It has been shown that the probability of error for the problem of terrain classification can be reduced when multiple independent measurements are possible [*Kong et al.*, 1988]. In this section, the four-look classification is achieved by treating the data from every four consecutive pixels in azimuth as four independent looks of one pixel. For the supervised classification, the distance measure of the combined pixel is the average of those of the original four pixels, whereas the unsupervised four-look classification is achieved by averaging the Mueller matrix over every four pixels in azimuth. It is found that this four-look classification greatly improves the probability of classification. The performances of the various supervised and unsupervised classification schemes for both single-look and four-look classification will then be compared in section 6.2c, and the results are summarized in section 6.2d.

a Supervised Classification Procedure

a.1 The Bayes classifier

In reviewing the Bayes Classifier, we first define a complex linear vector $\overline{X}$ containing a fully polarimetric radar return and call it the feature vector [*Kong et al.*, 1988].

$$\overline{X} = \begin{bmatrix} HH \\ HV \\ VV \end{bmatrix} = \begin{bmatrix} HH_I + i\, HH_Q \\ HV_I + i\, HV_Q \\ VV_I + i\, VV_Q \end{bmatrix} \tag{1}$$

where HH is the horizontally transmitted and received return, HV the cross polarized return, and VV the vertically transmitted and received return. The subscripts I and Q represent the in-phase and quadrature components. According to the Bayes maximum likelihood ratio test, [*Fukunaga,* 1972] the feature vector $\overline{X}$ will be assigned to the class ω_i if the probability of it being in that class is greater than that of it being in any other class. Mathematically, this can be written in the following form

$$\omega_i, \quad i = 1, 2, \ldots M \quad \text{classes}$$

$$\overline{X} \in \omega_i \quad \text{if} \quad \mathrm{P}(\omega_\mathrm{i}|\overline{\mathrm{X}}) > \mathrm{P}(\omega_\mathrm{j}|\overline{\mathrm{X}}) \quad \text{for all } \mathrm{j} \neq \mathrm{i} \tag{2}$$

However, if (2) is to be applied to radar data, reformulation of this criterion is necessary since one normally does not have, nor can easily assume the probability distribution over the range of classes for each pixel, $P(\omega_i|\overline{X})$. By using the Bayes theorem, the decision rule can be written in a more useful form as follows

$$\overline{X} \in \omega_i \quad \text{if} \quad \mathrm{P}(\overline{\mathrm{X}}|\omega_\mathrm{i})\mathrm{P}(\omega_\mathrm{i}) > \mathrm{P}(\overline{\mathrm{X}}|\omega_\mathrm{j})\mathrm{P}(\omega_\mathrm{j}) \quad \text{for all} \quad \mathrm{j} \neq \mathrm{i} \tag{3}$$

Classification can now be implemented with (3) as long as the *a priori* probabilities, $P(\omega_i)$ and the probability distribution of the radar returns for each class, $P(\overline{X}|\omega_i)$ are known. Since a forehand knowledge of the relative occurrence of each of the classes is not available, the *a priori* probabilities for all classes are assumed to be equal in all of the images discussed.

For convenience, the decision rule can be rewritten in terms of a distance measure defined to be the negative logarithm of the total probability.

$$\overline{X} \in \omega_i \quad \text{if} \quad \mathrm{d_i}(\overline{\mathrm{X}}) < \mathrm{d_j}(\overline{\mathrm{X}}) \quad \text{for all} \quad \mathrm{j} \neq \mathrm{i}$$

$$d_i(\overline{X}) = -\ln P(\overline{X}|\omega_i)P(\omega_i) \tag{4}$$

The classification is now based on minimum distance rather than maximum probability. This process of computing the distance measure for each class and assigning it to the class that yields the minimum distance is carried out pixel by pixel until all the pixels of the image are classified, resulting in a final false color-coded image. Likewise, the four-look classification is achieved by comparing the averaged distance measures over every four pixels in azimuth and classifying these four pixels into the class with minimum distance.

a.2 Fully polarimetric classification

For the unnormalized data, the polarimetric feature vector recorded by the SAR is defined to be of the form given by (1). As for the probability distribution of the radar returns, it is assumed that the in-phase and quadrature components of the feature vector $\overline{X}$ have equal variance and are independent zero-mean Gaussian distribution. Based upon the assumption made, the joint probability density function for the feature vector $\overline{X}$ is a multivariate complex Gaussian distribution [*Urkowitz,* 1980]. Therefore, its corresponding conditional PDF for the m-th class will be of the form

$$P(\overline{X}|m) = \frac{1}{\pi^3 \left|\overline{\overline{C}}_m\right|} \exp\left\{-\overline{X}^+ \cdot \overline{\overline{C}}_m{}^{-1} \cdot \overline{X}\right\} \tag{5}$$

where $\overline{\overline{C}} = \langle \overline{X}\, \overline{X}^+ \rangle|_{A_m}$ is a 3 by 3 complex covariance matrix of the zero-mean polarimetric data, i.e., $< \overline{X} >|_{A_m} = 0$. A_m represents the training area for the m-th class over which the covariance matrix is spatially averaged, as shown in Fig. 6.1. From the indicated regions the three covariance matrices are obtained which correspond to the three classes: ocean, urban, and park, considered in this image.

From the definition given in (4), the distance measure corresponding to the fully polarimetric classification can easily be obtained from the probability function in (5). Thus, the distance measure for the m-th class can be written as

$$d_m(\overline{X}) = \overline{X}^+ \cdot \overline{\overline{C}}_m{}^{-1} \cdot \overline{X} + \ln\left|\overline{\overline{C}}_m\right| - \ln[P_a(m)] \tag{6}$$

Any term of the distance measure that is not a function of m has been dropped since they do not contribute to the classification. In (6), it can be seen that the covariance matrix, which is obtained from the training regions, serves as a linear weighting vector for the polarimetric return power which optimizes classification.

Four-look Classification based on this distance measure (6) for classification is shown in Fig. 6.2, where the three classes: ocean, urban, and park are represented by the colors: blue, red, and green, respectively. Single-look classification is also implemented with the probability of error summarized in Table 6.1. Even with impure training regions for the park and urban classes, as can be seen in Fig. 6.1, classification

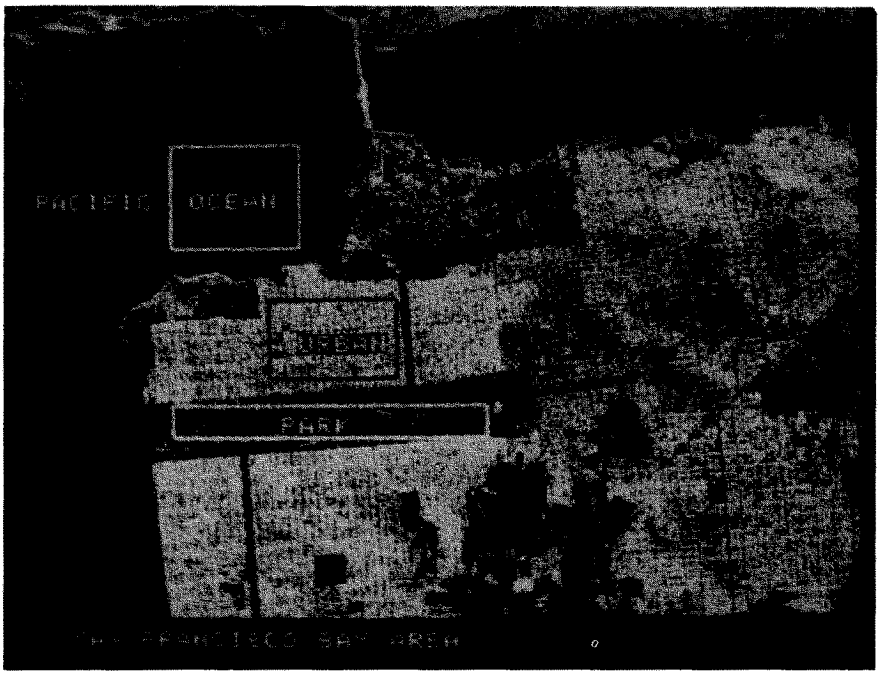

Figure 6.1 Training regions for the three classes: ocean, park, and urban selected from the San Francisco Bay area image to compute covariance matrices for supervised Bayes classification.

using the fully polarimetric information was able to correctly classify a large portion of the terrain components. This classifier was able to identify the tree-lined boulevards of San Francisco and even locate the small lakes within the Golden Gate Park. However, the upper right-hand region of the image was misclassified as urban region, though it should have been classified as ocean. This is due to the higher backscatter from the ocean surface in that region as can be seen in Fig. 6.1. One possible reason for this higher return is a smaller angle of incidence (closer to normal) in this region. This problem can be corrected by implementing a normalization technique which is presented next.

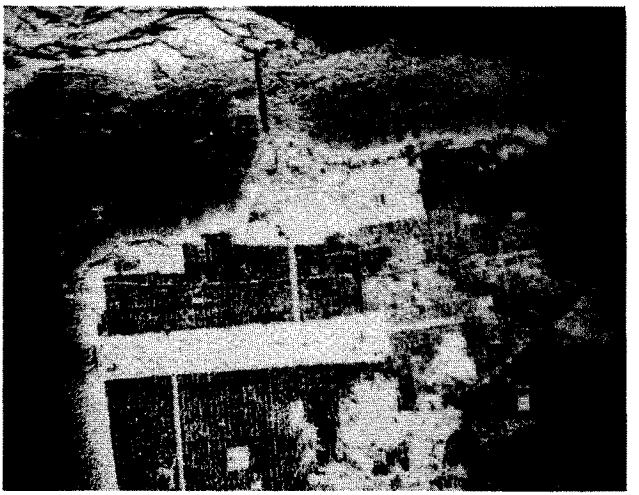

Figure 6.2 Supervised Bayes classification of San Francisco Bay area based on fully polarimetric data [see color plate 6.1].

a.3 Normalized polarimetric classification

When the absolute backscattered power is uncertain, classification can be based on a normalized feature vector given as

$$\frac{\overline{X}}{N} = \frac{1}{N}\begin{bmatrix} HH \\ HV \\ VV \end{bmatrix} \tag{7a}$$

$$N = \sqrt{|HH|^2 + |HV|^2 + |VV|^2} \tag{7b}$$

It has been shown that the classification scheme based on normalized polarimetric data is independent of the normalization function. This holds provided that the PDF of the normalized polarimetric data is derived from the same assumption used to derive the PDF of the unnormalized data [*Yueh et al.*, 1988].

A spherical transformation can be used for the Euclidean norm given in (7b) to derive the PDF of the normalized polarimetric data [*Yueh et al.*, 1988]. Assuming that the probability density for the unnormalized data is a multivariate complex Gaussian distribution, the

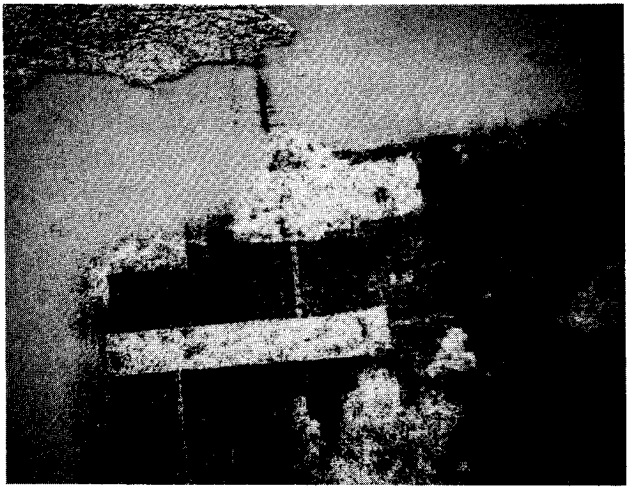

Figure 6.3 Bayes classification of San Francisco Bay area using normalized polarimetric data [see color plate 6.2].

PDF for the normalized data, written in terms of the new normalized quantities θ and ϕ is

$$P(\theta, \phi, \phi_{hh}, \phi_{hv}, \phi_{vv}|m) = \frac{\cos\phi \sin\phi \cos\theta \sin^3\theta}{\pi^3 \left|\overline{\overline{C}}_m\right|} \left(\frac{\overline{X}^+ \cdot \overline{\overline{C}}_m^{-1} \cdot \overline{X}}{N^2}\right)^{-3} \tag{8}$$

where

$$\theta = \cos^{-1}\left(\frac{|VV|}{N}\right) \tag{9a}$$

$$\phi = \tan^{-1}\left(\frac{|HV|}{|HH|}\right) \tag{9b}$$

From (8), the new distance measure for the normalized polarimetric case is then easily shown to be as follows

$$d_m = -\ln[P_a(m)] + \ln\left|\overline{\overline{C}}_m\right| + 3\ln\left(\overline{X}^+ \cdot \overline{\overline{C}}_m^{-1} \cdot \overline{X}\right) \tag{10}$$

Note that classification performance is independent of the normalization scheme since the normalization factor does not appear in the above expression.

By using the new distance measure given in (10), the same San Francisco Bay SAR image is classified into the ocean, urban, and park regions as shown in Fig. 6.3 for four-look classification. Again, it is assumed that the *a priori* probabilities of each class are equal. Note that the upper right-hand region of the image is now correctly classified as ocean. The result shown in Fig. 6.3 clearly indicates that the normalized polarimetric classification can be quite useful in regions where the absolute return is uncertain. However, it is observed that the performance in the urban-park region has been degraded. This is not surprising since the absolute levels of the radar returns are not used by this classifier.

The classification procedures were applied to another SAR image from a forested region near Traverse City, Michigan. This image was classified into regions consisting of corn fields, forest, lakes, and agricultural fields which are color-coded red, green, blue, and yellow, respectively. The training regions for these four classes are shown in Fig. 6.4, and the classified images for the fully polarimetric and normalized polarimetric classifiers are shown in Figs. 6.5 and 6.6, respectively. Note that these images are obtained using the four-look classification scheme described at the beginning of section 6.2. The classified images clearly indicate that the fully polarimetric result is much better than the normalized classification, unlike the San Francisco images, since there were no large misclassifications due to unusually high returns in the Traverse City fully polarimetric image.

a.4 Simple feature classification

Instead of using the fully polarimetric information, specific features can be isolated for classification by deriving the appropriate probability density functions. The results will then indicate the strong and weak points of each feature in the classification of earth terrain. To derive the classification procedures for simple features, the following

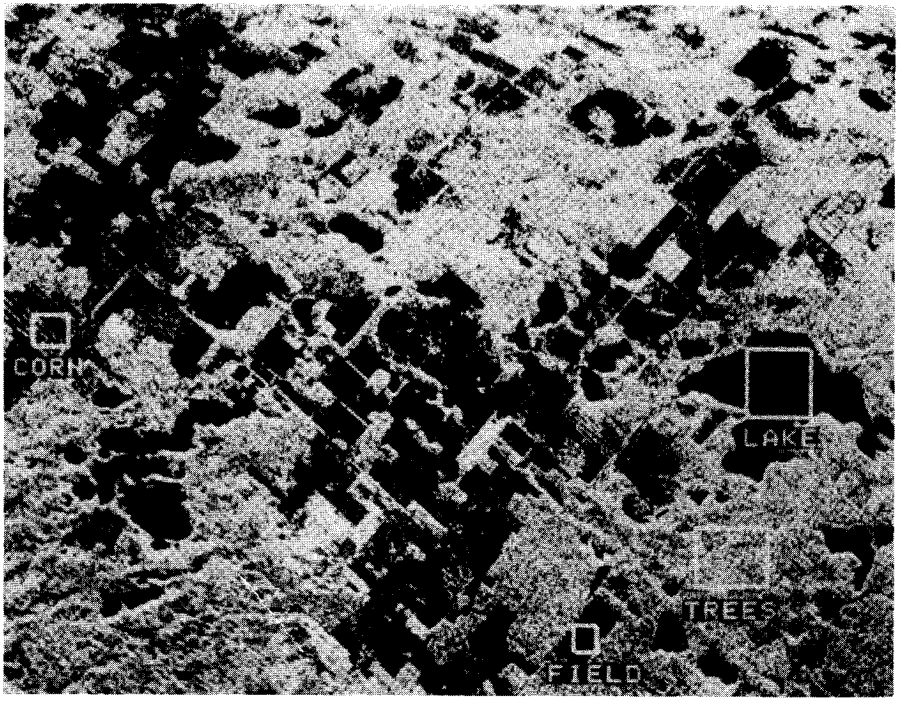

Figure 6.4 Training regions selected for the four classes: corn, fields, lake, and trees selected from the Traverse City, Michigan area image to compute covariance matrices for supervised Bayes classification.

general form of the polarimetric covariance matrix is assumed

$$\overline{\overline{C}}_m = \sigma_m \begin{bmatrix} 1 & \beta_m\sqrt{e_m} & \rho_m\sqrt{\gamma_m} \\ \beta_m^*\sqrt{e} & e_m & \xi_m\sqrt{\gamma_m e_m} \\ \rho_m^*\sqrt{\gamma_m} & \xi_m^*\sqrt{\gamma_m e_m} & \gamma_m \end{bmatrix} \tag{11}$$

where

$$\sigma_m = < |HH|^2 > |_{A_m} \tag{12a}$$

$$e_m = < |HV|^2 > |_{A_m}/\sigma_m \tag{12b}$$

$$\gamma_m = < |VV|^2 > |_{A_m}/\sigma_m \tag{12c}$$

$$\rho_m = \frac{< HH\ VV^* >|_{A_m}}{\sigma_m \sqrt{\gamma_m}} = |\rho_m| \exp\left[i\phi_{\rho_m}\right] \tag{12d}$$

$$\beta_m = \frac{< HH\ HV^* >|_{A_m}}{\sigma_m \sqrt{e_m}} = |\beta_m| \exp\left[i\phi_{\beta_m}\right] \tag{12e}$$

$$\xi_m = \frac{< HV\ VV^* >|_{A_m}}{\sigma_m \sqrt{e_m \gamma_m}} = |\xi_m| \exp\left[i\phi_{\xi_m}\right] \tag{12f}$$

The parameters ρ, β, and ξ are the complex correlation coefficients between the polarimetric channels, γ is the ratio of average VV power to the average HH power, and e is the depolarization ratio within the training region. From the multivariate Gaussian distribution assumption, the probability density functions corresponding to each simple feature can be derived.

For classification based solely on the absolute amplitude such as $|HH|$, $|HV|$, and $|VV|$, the Rayleigh distribution is applied [*Kong et al.*, 1988].

$$P(Y|m) = \frac{2Y}{\sigma_{y_m}} \exp\left[\frac{-Y^2}{\sigma_{y_m}}\right] \tag{13}$$

where $\sigma_{y_m} = \sigma_m$ for $Y = |HH|$, $\sigma_{y_m} = \sigma_m e_m$ for $Y = |HV|$, and $\sigma_{y_m} = \sigma_m \gamma_m$ for $Y = |VV|$.

Figure 6.7 illustrates the four-look classification based on the magnitude of the HH return for the San Francisco Bay area image. Although the performance is worse than that of the fully polarimetric classification, this feature yielded the best overall performance among the simple features considered. It should be noted that the same misclassification in the upper right-hand region occurred as was the case for the fully polarimetric image. This problem can be corrected by considering classification schemes based on normalized features such as the phase difference between receiver channels and normalized amplitude ratios.

To examine classification performance using simple normalized features, the PDFs for the magnitude ratios $|VV|/|HH|$ and $|HV|/|HH|$ need to be derived. It can be shown for the ratio $r = |VV|/|HH|$ that the PDF is [*Kong et al.*, 1988; *Kriegler et al.*, 1971]

$$P(r|m) = 2\gamma_m(1 - |\rho_m|^2)\frac{r(\gamma_m + r^2)}{[(\gamma_m + r^2)^2 - 4\gamma_m r^2|\rho_m|^2]^{3/2}} \tag{14}$$

By replacing $|\rho_m|$ with $|\beta_m|$ and γ_m with e_m, respectively, this expression is transformed into, the probability density for the ratio $r =$

Figure 6.5 Supervised Bayes classification of Traverse City, Michigan using fully polarimetric data [see color plate 6.3].

$|HV|/|HH|$.

The $|HV|/|HH|$ four-look classified image (Fig. 6.8) shows many interesting features. For instance, if observed carefully, the trees lining the large boulevards of San Francisco can be seen. Trees in the other parts of the image are classified well, although the classifier had some difficulty separating the urban and ocean regions. The results indicate that the depolarization ratio is a good discriminate for identifying trees. Also, the essential character of this image resembles the coefficient of variation image [*van Zyl et al.*, 1987] obtained by displaying, in grey-levels, the ratio of the minimum to maximum co-polarized power.

The PDF of the phase difference between HH and VV returns is found by integrating the joint Gaussian PDF for the fully polarimetric data over the amplitudes and the phase of the HV return, ϕ_{hv}. It is given as [*Kong et al.*, 1988]

$$P(\phi|m) = \frac{(1-|\rho_m|^2)}{2\pi}\left[\frac{(1-\chi_m^2)^{1/2}+\chi_m(\pi-\cos^{-1}\chi_m)}{(1-\chi_m^2)^{3/2}}\right] \qquad (15)$$

Figure 6.6 Supervised Bayes classification of Traverse City, Michigan using normalized polarimetric data [see color plate 6.4].

where

$$\phi = \phi_{hh} - \phi_{vv} \tag{16a}$$

$$\chi_m = |\rho_m| \cos(\phi - \phi_{\rho_m}) \tag{16b}$$

This PDF can be modified to handle the phase difference between HH and HV, in addition to phase difference between HV and VV returns by using the transformation $|\rho_m| \to |\beta_m|$, $\phi_{\rho_m} \to \phi_{\beta_m}$ for $\phi = \phi_{hh} - \phi_{hv}$ and $|\rho_m| \to |\xi_m|$, $\phi_{\rho_m} \to \phi_{\xi_m}$ for $\phi = \phi_{hv} - \phi_{vv}$ responses, respectively.

Four-look classification based on the phase difference between the HH and VV channels is shown in Fig. 6.9. The performance in the ocean is very good, whereas the results in the urban-park region are clearly worse than that of the $|HH|$ classified image. Class distinction in this image can be improved, especially in the urban-park region, by preserving the grey-levels of the $|HH|$ image when color coding. The result is shown in Fig. 6.10. The performance is much better now since, in a sense, classification is based on both the magnitude and phase information.

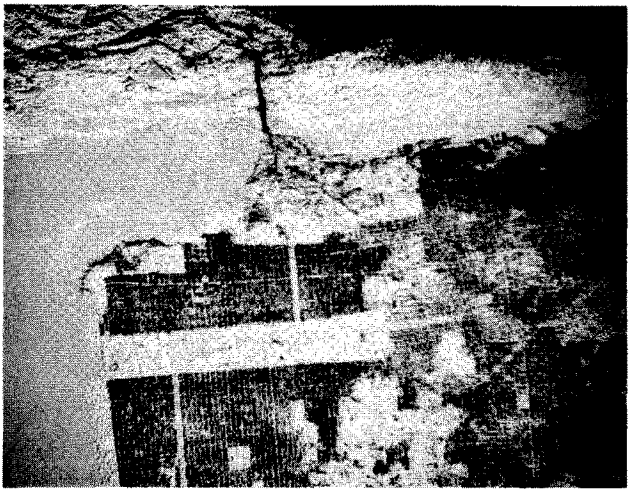

Figure 6.7 Supervised Bayes classification of San Francisco Bay area using $|HH|$ amplitude information only [see color plate 6.5].

b. Unsupervised Classification Procedure

The unsupervised classification procedure utilizes a somewhat simpler approach than the Bayes procedure described previously. This classification technique is based on comparing the general properties of the Stokes parameters of the scattered wave to that of some simple scattering models. The algorithm classifies scatterers based on the relationship between the orientation angles and handedness of the transmit polarization ellipse to the corresponding parameters of the scattered wave for every transmit polarization ellipse.

For example, a slightly rough dielectric surface scattering model [*Rice,* 1951] predicts that the measured HH and VV signals will be in-phase, and the orientation angle of the scattered wave polarization ellipse increases as the orientation angle of the transmitted wave polarization ellipse increases and decreases as the orientation angle of the transmitted wave polarization ellipse decreases; i.e., the orientation angle of the scattered wave polarization ellipse tracks that of the transmitted wave polarization ellipse. However, the handedness of the scattered wave polarization will be opposite to that of the transmit-

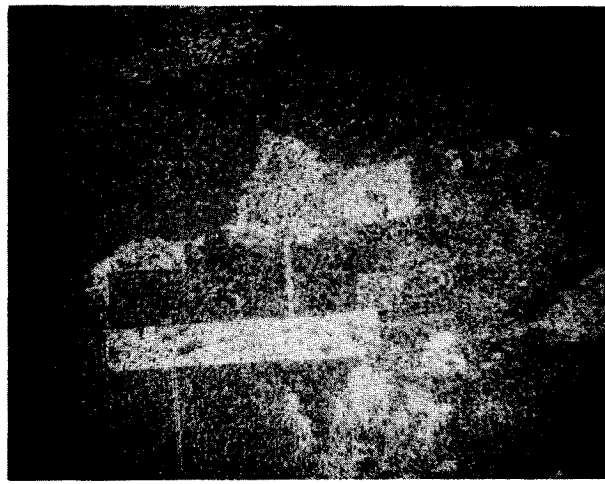

Figure 6.8 Supervised Bayes classification of San Francisco Bay area using magnitude ratio $|HV|/|HH|$ [see color plate 6.6].

ted wave polarization; for example, a left-handed elliptical transmitted polarization will be returned as a right-handed elliptical polarization.

A dihedral corner reflector, on the other hand, exhibits a double bounce geometry [*van Zyl et al.*, 1987], resulting in a 180° phase difference between the measured HH and VV signals. In this case, the orientation angle of the scattered wave polarization ellipse decreases as the orientation angle of the transmitted wave polarization ellipse increases and increases as the orientation angle of the transmitted wave polarization ellipse decreases. The handedness of the scattered wave polarization in this case is the same as that of the transmitted wave polarization.

For areas which exhibit multiple interactions, we have observed a different behavior. As in the case of a slightly rough dielectric surface, the orientation angle of the scattered wave tracks that of the transmitted wave polarization ellipse. The handedness of the scattered wave, however, is the same as that of the transmitted wave polarization which is more consistent with a double bounce mechanism. This behavior can also be generated by a class of vegetation models [*Richards et al.*, 1987;

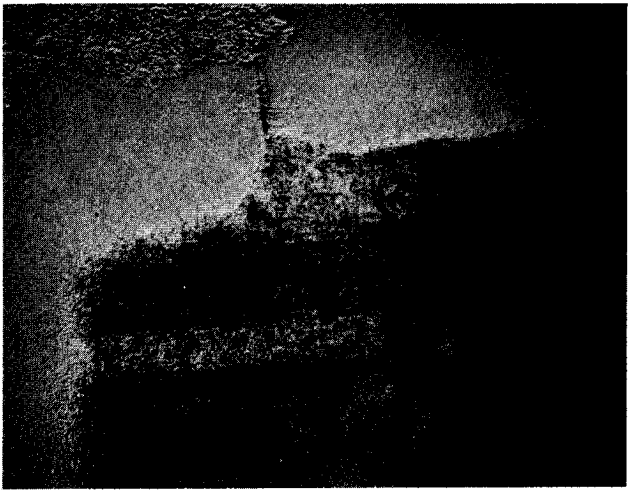

Figure 6.9 Supervised Bayes classification of San Francisco Bay area using phase difference $\phi_{hh} - \phi_{vv}$ [see color plate 6.7].

van Zyl et al., 1987] or a rough surface partially covered with blocky boulders [*van Zyl et al.*, 1987].

The unsupervised algorithm classifies each pixel of the image by comparing its polarimetric properties to the various models for selected transmitting polarization states. It then assigns the pixel to the class which exhibits similar scattering properties as one of these models. If the pixel does not exhibit polarimetric properties consistent with that predicted by any one of the three models, it is labelled as *unable to be classified.* The classification algorithm produces a false color-coded image as output. The color assignments are as follows: pixels having scattering characteristics consistent with the rough surface model are color-coded blue; those similar to the dihedral corner reflector model are color-coded red; diffusely scattering areas are color-coded green; and pixels that do not exhibit any of the models' scattering characteristics are color-coded yellow. Notice that this classification algorithm does not use training areas, and hence the terminology, unsupervised classification.

For the four-look unsupervised classification, the averaged Mueller

Figure 6.10 Supervised Bayes classification of San Francisco Bay area using phase difference $\phi_{hh} - \phi_{vv}$ color-coded by incorporating grey-levels of the $|HH|$ return power [see color plate 6.8].

matrices of every four pixels are classified based on the single-look classification procedure. Figure 6.11 shows the classified image of the San Francisco Bay area when the four-look unsupervised classification procedure was applied. As was the case in Fig. 6.10 for classification based on the phase difference, the intensity of the HH return power is preserved when color-coding. It is clear that, in general, pixels in the ocean area were correctly classified as being consistent with the rough surface model; while most pixels in the urban, as well as the lighthouse in the ocean (visible off the northwest corner of San Francisco), were correctly classified as being similar to the dihedral corner reflector model. Most of the pixels in Golden Gate park and other tree-covered parts of the city, including the wider tree-lined streets, were classified as being similar to areas with a large amount of diffuse scattering, as predicted by the forested areas model. Notice the urban area which shows up as a green triangle on the right-hand part of the image. Even though there are very few trees in this part of San Francisco, the algorithm classified this urban area as exhibiting a large amount of diffuse scattering. The explanation for this lies in the fact that the streets in this

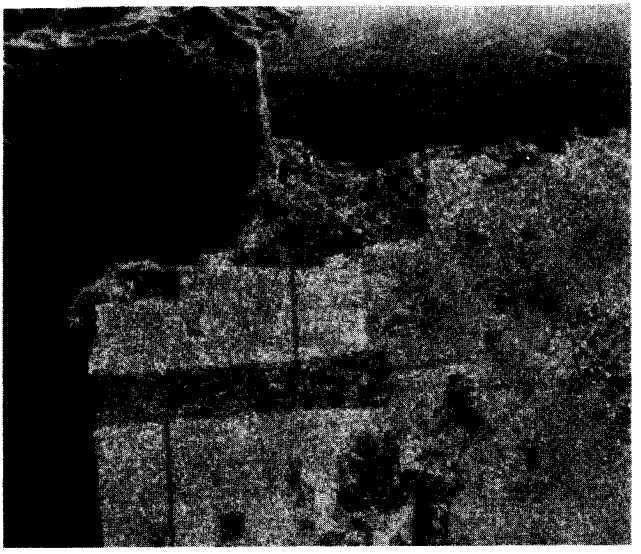

Figure 6.11 Unsupervised classification based on simple models of San Francisco Bay area incorporating grey-levels of the $|HH|$ return power [see color plate 6.9].

part of the city are at an angle of about 45° with respect to the radar look direction, which leads to a scattering mechanism similar to that described for a rough surface partially covered with blocky boulders.

The unsupervised classification algorithm was also applied to the Traverse City, Michigan data previously discussed. This area consists of forested areas, agricultural fields, and lakes. The results of the four-look unsupervised classification algorithm, when applied to this image, are shown in Fig. 6.12. All the lakes are correctly classified as areas which have polarization characteristics similar to those predicted by slightly rough surface scattering, while the forested areas are classified as exhibiting a large amount of diffuse scattering. Most of the agricultural fields are classified as having polarization characteristics similar to those predicted by the slightly rough surface model. Notice that the far-range shores of the lakes are classified as double bounce reflectors, which is due to scattering off the lake surface into the trees on the shore and back to the radar or vice versa. Also notice that some of the agricultural fields (for example the ones denoted (1) and (2) in Fig. 6.12) are classified as a combination of single and double reflections.) Most

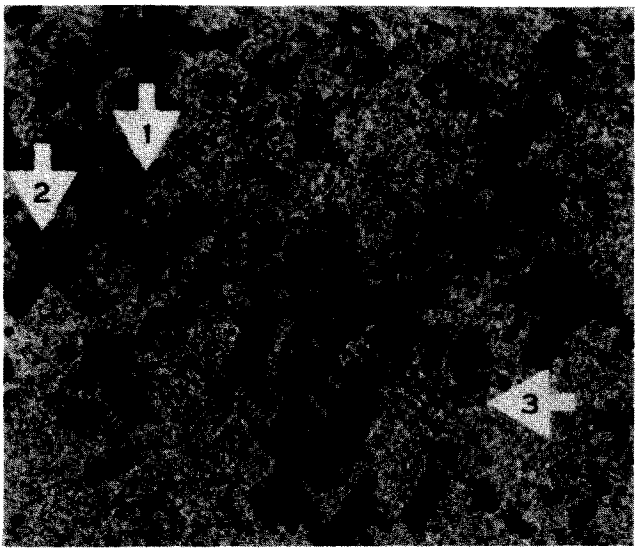

Figure 6.12 Unsupervised classification based on simple models of Traverse City, Michigan incorporating grey-levels of the $|HH|$ return power [see color plate 6.10].

of these fields are corn fields. Corn fields exhibit phase differences between the HH and VV signals which may be appreciably different from the 0° predicted by the slightly rough surface model or the 180° predicted by the dihedral corner reflector model. The area labeled (3) in Fig. 6.12 is classified as exhibiting double reflections. This area consists mostly of trunks of dead trees standing on water-saturated ground resulting in a strong doubly reflected component in the return signal. This example shows that in some cases even this simple classification algorithm is capable of distinguishing between scattering by healthy forests and areas where the trees are dead.

c. Classification Error Analysis

In order to quantitatively assess the relative performance of the classifiers discussed, the probability of error is computed by taking the training regions as absolute ground truth and counting the misclassification within those regions. Table 6.1 shows the results of this analysis for the single-look classification of the fully polarimetric image of the

San Francisco Bay area. The probability of error shown in the last column is obtained by dividing the total number of misclassifications by the total number of pixels in each training region. Then the average probability of error is computed by averaging the three probabilities obtained for each class. In the same way, the results for the four-look classification are shown in Table 6.2 (Note that the total number of pixels is reduced by a factor of four as a result of the four-look averaging.) Carrying out this procedure for each of the features considered, we obtain the numbers compiled in Table 6.3. For the unsupervised technique, two different probabilities of error are computed depending on how the unclassified pixels are accounted for. In case (a), the unclassified pixels were ignored and not included when computing the error; whereas in case (b), the unclassified pixels were counted with the misclassified pixels. The numbers show that the fully polarimetric classification gives the optimal result. The phase difference Bayes classification and the unsupervised classification, which are both two feature classifications, gave similar performance. It should be noted that this may not be the most accurate way of comparing the unsupervised and supervised classifications since the unsupervised technique did not make use of the information contained in the training regions. However, comparison among the supervised classification gives a good measure of the relative performance for each feature; although in the absolute sense, the probability of error may be higher since the training regions may not be pure according to real ground truth. A much better comparison would be to calculate the probability of error over the entire image with respect to the actual pixel by pixel ground truth at the time of the measurement; however, no such information was available.

Classified Training	Urban	Park	Ocean	P_{error}
Urban	32391	29044	581	0.478
Park	5150	39512	2802	0.168
Ocean	43	1361	60548	0.023

Avg. $P_{\text{error}} = .223$

Table 6.1 Single-look classification errors and probability of errors obtained for the fully polarimetric San Francisco image by counting the misclassification within each training region assumed to be of a single class.

d. Summary

Two methods for classifying fully polarimetric SAR data, i.e., supervised Bayes classification and an unsupervised classification technique, have been presented and applied to the SAR images of the San Francisco Bay area and a forested area near Traverse City, Michigan. Both techniques can be utilized to full advantage by employing the most appropriate algorithm for a particular application. When accurate training data are available, Bayesian classification will yield optimal results; whereas in the case where ground truth is not well known, unsupervised classification will be useful. In either case, the need for photointerpretation is minimized by employing these polarimetric terrain classification algorithms.

Classified Training	Urban	Park	Ocean	P_{error}
Urban	9477	6027	0	0.389
Park	975	10823	102	0.095
Ocean	24	208	15256	0.015

Avg. $P_{\text{error}} = .165$

Table 6.2 Four-look classification errors and probability of errors obtained for the fully polarimetric San Francisco image by counting the misclassification within each training region assumed to be of a single class.

Feature	Avg. P_{error} (Single-look)	Avg. P_{error} (Four-look)
Fully Polarimetric	0.223	0.165
Normalized Polarimetric	0.301	0.183
Magnitude of $\|HH\|$	0.383	0.270
Phase Difference $\phi_{hh} - \phi_{vv}$	0.415	0.312
Simple Models (a)	0.437	0.342
Magnitude Ratio $\|HV\|/\|HH\|$	0.529	0.366
Simple Models (b)	0.516	0.394

Table 6.3 Average Probability of Errors for the supervised and unsupervised classification of San Francisco Images. Fully polarimetric Bayes classification gives the minimum probability of error.

6.3 Maximum Contrast Enhancement

In this section a systematic approach is presented for obtaining the optimal polarimetric matched filter, i.e., that filter which produces maximum contrast between two scattering classes. The contrast ratio is defined as a function of a linear weighting vector (polarization filter) and the polarimetric covariance matrices of the two classes. To exhibit the physical significance of this filter, it is transformed into its associated transmitting and receiving polarization states, written in terms of horizontal and vertical vector components.

In section 6.3a, the polarimetric matched filter and the contrast ratio are defined. The method for achieving maximum contrast between classes, as well as a closed form solution to this problem for the case in which the polarimetric covariance matrices contain four zero elements is considered in section 6.3b. The maximization procedure involves solving an eigenvalue problem where the eigenvector corresponding to the maximum contrast ratio is the optimal polarimetric matched filter. It is then shown how to realize the polarimetric matched filter in terms of an equivalent transmitting and receiving polarization pair. In section 6.3c, for the special case where the transmitting polarization is fixed, the receiving polarization which maximizes the contrast ratio is also obtained. Discussion of the results obtained using optimal polarimetric matched filtering is the scope of section 6.3d. Polarimetric filtering is applied to SAR images obtained from the Jet Propulsion Laboratory. It is shown, both numerically and through the use of radar imagery, that maximum image contrast can be realized when data are processed with the optimal polarimetric matched filter.

a. Polarimetric Matched Filter and Contrast Ratio

Assume that two classes of statistically distributed scattering types exist. Each class is represented by a covariance matrix of the form $\overline{\overline{C}}_j = E\left[\overline{X}\,\overline{X}^{\dagger}\right]_j$ where $j = a, b$ represents class A and class B scatterers, respectively. Here $E[\cdot]$ denotes the expected value and superscript $\dagger$, the complex conjugate transpose operation. For the case of electromagnetic waves which are backscattered from a reciprocal media, $HV = VH$. Therefore, the polarimetric feature vector, $\overline{X}$, is expressed in a horizontal-vertical polarization basis as (1) [*Kong et al., 1988*].

The objective is to find the best linear weighting vector or polarimetric matched filter for processing an observed polarimetric feature vector; that is, the linear combination

$$Y = \overline{W}^{\dagger}\,\overline{X} \tag{17}$$

where

$$\overline{W} = \begin{bmatrix} W_{hh} \\ W_{hv} \\ W_{vv} \end{bmatrix} \tag{18}$$

which provides the maximum contrast ratio, r, between the two respective classes (class A and class B). The maximum contrast ratio is defined as

$$r = \mathrm{MAX}\left\{\mathrm{MAX}_{\overline{W}}(r_{ab}), \mathrm{MAX}_{\overline{W}}(r_{ba})\right\} \tag{19}$$

where

$$r_{ab} = \frac{\overline{W}^{\dagger}\,\overline{\overline{C}}_a\,\overline{W}}{\overline{W}^{\dagger}\,\overline{\overline{C}}_b\,\overline{W}} \tag{20a}$$

$$r_{ba} = \frac{\overline{W}^{\dagger}\,\overline{\overline{C}}_b\,\overline{W}}{\overline{W}^{\dagger}\,\overline{\overline{C}}_a\,\overline{W}} \tag{20b}$$

Note that from a physical point of view, the elements of the vector $\overline{W}$ in (17) are linear weighting coefficients which adjust the amplitude and phase of the polarimetric radar measurements. In (20a), the term r_{ab} denotes the contrast ratio of class A with respect to class B scatterers. The contrast ratio of class B with respect to class A scattering elements is expressed in (20b) as r_{ba}. The symbol $\mathrm{MAX}\{\cdot\}$ signifies the maximum value of the argument, i.e., either r_{ab} or r_{ba} in this case, whereas $\mathrm{MAX}_{\overline{W}}(r_{ab})$ indicates that a linear weighting vector W has been obtained which maximizes r_{ab} independently of r_{ba}, and $\mathrm{MAX}_{\overline{W}}(r_{ba})$ implies that a different linear weighting vector has been found which maximizes r_{ba} independently of r_{ab}. Also, the numerator and denominator in (20a) and (20b) are obtained from (17) by taking the expected value of the return power from each class.

To demonstrate that the polarimetric matched filter, $\overline{W}$, directly corresponds to specific transmitting and receiving polarizations, we express (17) in terms of a monostatic reciprocal scattering matrix as

$$Y = [H_r \quad V_r] \begin{bmatrix} HH & HV \\ HV & VV \end{bmatrix} \begin{bmatrix} H_t \\ V_t \end{bmatrix} \tag{21}$$

in which the values H_t and V_t , H_r and V_r represent the horizontal and vertical vector components of the transmitting and receiving polarization state, respectively. Also, without loss of generality, it is assumed that

$$|H_t|^2 + |V_t|^2 = 1 \tag{22a}$$

$$|H_r|^2 + |V_r|^2 = 1 \tag{22b}$$

Equating (17) and (21) yields

$$H_t H_r = W_{hh}^* \tag{23a}$$

$$H_t V_r + V_t H_r = W_{hv}^* \tag{23b}$$

$$V_t V_r = W_{vv}^* \tag{23c}$$

Thus, given a general linear weighting vector, $\overline{W}$, its corresponding polarization state components, H_t, V_t, H_r, and V_r, can be completely specified through (23). This will be shown in section 6.3b.

Note that (21) indicates the transmitting and receiving polarization vectors are reciprocal, i.e., the terms H_t and V_t can be interchanged with H_r and V_r without altering the measurement, Y. Therefore, in the case of reciprocal backscattering, the same contrast ratio will be obtained if the transmitting and receiving polarization vectors are exchanged.

b. Optimal Polarimetric Matched Filter Required to Obtain Maximum Contrast Between Two Scattering Classes

b.1 Solution of optimal polarimetric matched filter

In order to compute the optimal polarimetric matched filter, (20a) and (20b) must be maximized. The linear weighting vector which corresponds to the maximum contrast ratio, shown in (19), will be denoted as the optimal polarimetric matched filter. The maximization procedure makes use of the Lagrange multiplier technique. Details of this procedure were outlined by *Cadzow* [1980], although the steps will be repeated here for completeness. For example, in order to maximize r_{ab}, in (20a),

$$\text{MAX}\left\{\overline{W}^{\dagger}\,\overline{\overline{C}}_a\,\overline{W}\right\} \tag{24}$$

is determined under an arbitrary constraint

$$\overline{W}^{\dagger}\,\overline{\overline{C}}_b\,\overline{W} = 1 \tag{25}$$

This reformulation is possible, without loss of generality, since the linear weighting vector can be multiplied by any arbitrary complex constant without affecting the contrast ratio. The solution to this constrained maximization problem is obtained by making use of the Lagrange multiplier concept, which reflects the constraint shown in (25). Its solution will be a stationary point of the auxiliary functional

$$f(\overline{W}) = \overline{W}^{\dagger}\,\overline{\overline{C}}_a\,\overline{W} + \lambda\left[1 - \overline{W}^{\dagger}\,\overline{\overline{C}}_b\,\overline{W}\right] \tag{26}$$

in which λ is a scalar valued Lagrange multiplier. Specifically, the stationary points of this auxiliary functional are found first by representing the generally complex vector $\overline{W}$ in terms of its real and imaginary components, as $\overline{W}_R + i\,\overline{W}_I$. Then, taking the gradient of the auxiliary functional with respect to $\overline{W}_R$ and $\overline{W}_I$, setting the resulting equations equal to zero, i.e.,

$$\frac{\partial f(\overline{W})}{\partial \overline{W}_R} = 0 \tag{27a}$$

$$\frac{\partial f(\overline{W})}{\partial \overline{W}_I} = 0 \tag{27b}$$

yields the necessary condition for a maxima or minima to occur. Carrying out (27a) and (27b) leads to the eigenvalue equation

$$\overline{\overline{C}}_a\,\overline{W} = \lambda\,\overline{\overline{C}}_b\,\overline{W} \tag{28}$$

Note that the eigenvalue (Lagrange multiplier) λ, in (28), is the contrast ratio r_{ab} given by (20a), whereas $1/\lambda$ signifies the contrast ratio r_{ba} shown in (20b). Since the objective is to determine the maximum contrast ratio between classes, the values of the maximum and the reciprocal of the minimum eigenvalue must be compared and the larger of the two selected. The eigenvector which corresponds to this maxima is the optimal polarimetric matched filter that should be employed to process the radar polarimetry. Note that it is not required to maximize both (20a) and (20b). By extremizing (20a) then selecting the largest of either the maximum eigenvalue or the reciprocal of the minimum eigenvalue, both (20a) and (20b) have been simultaneously maximized.

In the event that the eigenvalues of (28) are degenerate, there will exist no preferred polarization basis for which the expected power return of two objects can be separated. Assuming then, that the contrast

ratios are not degenerate, the optimal polarimetric matched filter, $\overline{W}$, is interpreted to be the equivalent transmitting and receiving polarization state which a radar can utilize in order to detect the maximum contrast, or separation in average intensity, between classes.

The contrast optimization approach used for the case of a monostatic radar also can be applied to a polarimetric bistatic radar. Taking into account the fact that for bistatic scattering $HV \neq VH$ when defining $\overline{X}$ and $\overline{W}$ in (1) and (17), leads to 4×4 polarimetric covariance matrices which characterize the scattering classes. Then applying exactly the same method of solution yields the transmitting and receiving polarization state that maximizes contrast between scattering classes.

Once the optimal polarimetric matched filter is obtained, the corresponding transmitting and receiving polarization state can be calculated. Without loss of generality, the case when W_{hh} is not equal to zero will be shown. From (22) and (23), it is found that

$$H_t = \left[\left| \frac{W_{hv}^* \pm \sqrt{(W_{hv}^*)^2 - 4(W_{hh}W_{vv})^*}}{2W_{hh}^*} \right|^2 + 1 \right]^{-1/2} \tag{29a}$$

$$V_t = H_t \cdot \left[\frac{W_{hv}^* \pm \sqrt{(W_{hv}^*)^2 - 4(W_{hh}W_{vv})^*}}{2W_{hh}^*} \right] \tag{29b}$$

$$H_r = \frac{\tau}{H_t} \cdot W_{hh}^* \tag{29c}$$

$$V_r = \frac{\tau}{H_t} \cdot \left[\frac{W_{hv}^* \mp \sqrt{(W_{hv}^*)^2 - 4(W_{hh}W_{vv})^*}}{2} \right] \tag{29d}$$

where

$$\tau = \frac{1}{\sqrt{\tau_1 \cdot \tau_2 \cdot \tau_3}} \tag{30}$$

$$\tau_1 = |W_{hh}^*|^2 \tag{31a}$$

$$\tau_2 = 1 + \left| \frac{W_{hv}^* \mp \sqrt{(W_{hv}^*)^2 - 4(W_{hh}W_{vv})^*}}{2W_{hh}^*} \right|^2 \tag{31b}$$

$$\tau_3 = 1 + \left| \frac{W_{hv}^* \pm \sqrt{(W_{hv}^*)^2 - 4(W_{hh}W_{vv})^*}}{2W_{hh}^*} \right|^2 \tag{31c}$$

The absolute intensity value, I, is given by

$$I = \left| \tau \, \overline{W}^{\dagger} \, \overline{X} \right|^2 \tag{32}$$

where τ is the amplitude normalization constant given in (30).

The observed sign change in (29), i.e., $\pm$ or $\mp$, indicates the reciprocity of the transmitting and receiving polarization state, as previously mentioned. Also, the resulting transmitting and receiving polarization state is independent of any multiplicative constant effecting the matched filter. This is necessary since the general complex eigenvector solution to (28) can vary by a multiplicative complex constant; however, the resulting polarization state remains unaffected since this constant can be factored out.

Finally, a comparison between the methods for contrast enhancement presented in this chapter versus that originally proposed by *Ioannidis and Hammers* [1979] is in order. In their method, the target-to-clutter ratio was maximized to determine the optimal transmitting and receiving antenna Stokes polarization vectors. The *Ioannidis and Hammers'* method requires the use of three constraints in order to solve the maximization problem. One is similar to (25) in that it constrains the denominator of the target-to-clutter ratio to be equal to an arbitrary constant. The other two constrain the transmitting and receiving vectors to be antenna Stokes polarization vectors. This results in complex expressions which specify the optimal transmitting and receiving polarization state. In addition, they do not obtain the matched filter which corresponds to the optimal transmitting and receiving polarization state. When using *Cadzow's* method, only one constraint (25) is needed to solve for the optimal polarimetric matched filter. In this case, the maximization procedure only requires solving the eigenvalue problem shown in (28). It should be pointed out that both methods yield identical results when polarimetric target and clutter classes are prespecified.

The major difference between these two techniques is that *Ioannidis and Hammers'* method dealt with the specific problem of maximizing the target-to-clutter ratio by determining the optimal transmitting and receiving antenna Stokes polarization vectors, whereas the matched filtering approach used in this chapter can be applied to a more general class of problems. That is, *Cadzow's* procedure extends to multichannel, multifrequency sensor data. Polarimetric contrast enhancement is considered here as a special case.

b.2 Solution for the case of a covariance matrix with four zero elements

Thus far, the most general form of the polarimetric covariance matrix has been assumed, which is

$$\overline{\overline{C}}_j = \sigma_j \begin{bmatrix} 1 & \beta_j\sqrt{e_j} & \rho_j\sqrt{\gamma_j} \\ \beta_j^*\sqrt{e_j} & e_j & \xi_j\sqrt{e_j\gamma_j} \\ \rho_j^*\sqrt{\gamma_j} & \xi_j^*\sqrt{e_j\gamma_j} & \gamma_j \end{bmatrix} \tag{33}$$

where $j = a, b$ represents the class A and class B parameters, respectively, and

$$\sigma = \sigma_{hh} \tag{34a}$$

$$e = \sigma_{hv}/\sigma \tag{34b}$$

$$\gamma = \sigma_{vv}/\sigma \tag{34c}$$

$$\rho = \frac{E[HH \cdot VV^*]}{\sigma\sqrt{\gamma}} = |\rho| \exp(i\phi_\rho) \tag{34d}$$

$$\beta = \frac{E[HH \cdot HV^*]}{\sigma\sqrt{e}} = |\beta| \exp(i\phi_\beta) \tag{34e}$$

$$\xi = \frac{E[HV \cdot VV^*]}{\sigma\sqrt{e\gamma}} = |\xi| \exp(i\phi_\xi) \tag{34f}$$

Here, the values σ_{hh}, σ_{hv}, and σ_{vv} denote the normalized backscatter cross section per unit area of the HH, HV, and VV returns [*Kong et al.*, 1988].

It has been rigorously shown using the random medium model [*Borgeaud et al.*, 1987], that when each of the two scattering classes can be modeled as a uniform terrain cover, no average correlation exists between HH and HV returns, or between VV and HV returns. Therefore, the variables β and ξ, in (14), are both equal to zero; and the polarimetric covariance matrices contain four zero elements. This implies that the terrain exhibits azimuthal symmetry from a statistical point of view. It should be pointed out that this effect has been experimentally observed at various sites by MIT Lincoln Laboratory in their polarimetric measurements at 35 GHz [*Borgeaud et al.*, 1987] (see Table 6.5). In this case, the polarimetric covariance matrix can be

expressed as

$$\overline{\overline{C}}_j = \sigma_j \begin{bmatrix} 1 & 0 & \rho_j\sqrt{\gamma_j} \\ 0 & e_j & 0 \\ \rho_j^*\sqrt{\gamma_j} & 0 & \gamma_j \end{bmatrix} \tag{35}$$

A closed form solution to the general eigenvalue problem in (28), based on the covariance matrix in (35), is presented in the following. First, the eigenvalues for the matrix $\overline{\overline{C}}_b^{-1}\,\overline{\overline{C}}_a$ are determined. They can be expressed as

$$\lambda_1 = \frac{e_a\sigma_a}{e_b\sigma_b} \tag{36a}$$

$$\lambda_{2,3} = \frac{\sigma_a}{2\sigma_b\gamma_b\left(1-|\rho_b|^2\right)} \times \left[\gamma_a+\gamma_b-2\sqrt{\gamma_b\gamma_a}\,|\rho_a|\,|\rho_b|\cos\left(\phi_{\rho_a}-\phi_{\rho_b}\right) \pm \sqrt{\left[\gamma_a+\gamma_b-2\sqrt{\gamma_b\gamma_a}\,|\rho_a|\,|\rho_b|\cos\left(\phi_{\rho_a}-\phi_{\rho_b}\right)\right]^2 - 4\gamma_a\gamma_b\left(1-|\rho_b|^2\right)\left(1-|\rho_a|^2\right)}\right] \tag{36b}$$

Their corresponding eigenvectors are given as

$$\lambda_1 \rightarrow \overline{W}_1 = \begin{bmatrix} 0 \\ 1 \\ 0 \end{bmatrix} \tag{37a}$$

$$\lambda_{2,3} \rightarrow \overline{W}_{2,3} = \begin{bmatrix} 1 \\ 0 \\ \Upsilon_{2,3} \end{bmatrix} \tag{37b}$$

where

$$\Upsilon_{2,3} = \frac{\left[\gamma_a-\gamma_b-i\,2\sqrt{\gamma_b\gamma_a}\,|\rho_a|\,|\rho_b|\sin\left(\phi_{\rho_a}-\phi_{\rho_b}\right) \pm \sqrt{\left[\gamma_b+\gamma_a-2\sqrt{\gamma_b\gamma_a}\,|\rho_a|\,|\rho_b|\cos\left(\phi_{\rho_a}-\phi_{\rho_b}\right)\right]^2 - 4\gamma_a\gamma_b\left(1-|\rho_b|^2\right)\left(1-|\rho_a|^2\right)}\right]}{2\left(\gamma_b\sqrt{\gamma_a}\rho_a-\gamma_a\sqrt{\gamma_b}\rho_b\right)} \tag{38}$$

As in the case of the generalized solution, the eigenvector corresponding to the maximum of either the largest or the reciprocal of the smallest eigenvalue in (36) will produce maximum contrast between the two classes. Therefore, this eigenvector will be the optimal polarimetric matched filter which should be utilized to process the polarimetric feature vector.

c. *The Optimal Receiving Polarization State for a Fixed Transmitting Polarization*

If presented with a situation where the radar transmitting polarization state is fixed, an optimal receiving polarization state can be determined which maximizes the contrast between the two classes. This problem arises in the case of radar systems which are not fully polarimetric, i.e., they transmit using only a single polarization, say horizontal, but receive the principle and cross-polarization components of the scattered response, say the horizontal and vertical returns. Applying the following technique will indicate how to coherently combine the horizontal and vertical returns such that the contrast between classes is maximized.

Assume that the values H_t and V_t are known and that the requirement shown in (22a) is satisfied. Thus, from (23), $\overline{W}$ may be written as

$$\overline{W} = \begin{bmatrix} (H_t H_r)^* \\ (H_t V_r)^* + (V_t H_r)^* \\ (V_t V_r)^* \end{bmatrix} = \begin{bmatrix} H_t^* & 0 \\ V_t^* & H_t^* \\ 0 & V_t^* \end{bmatrix} \begin{bmatrix} H_r^* \\ V_r^* \end{bmatrix} = \zeta\, \overline{R} \tag{39}$$

Substituting (39) for $\overline{W}$ in (20a) gives

$$r_{ab} = \frac{\overline{R}^{\dagger}\, \overline{\overline{Z}}_a\, \overline{R}}{\overline{R}^{\dagger}\, \overline{\overline{Z}}_b\, \overline{R}} \tag{40}$$

where

$$\overline{\overline{Z}}_a = \zeta^{\dagger}\, \overline{\overline{C}}_a\, \zeta \tag{41a}$$

$$\overline{\overline{Z}}_b = \zeta^{\dagger}\, \overline{\overline{C}}_b\, \zeta \tag{41b}$$

Since $\overline{\overline{Z}}_a$ and $\overline{\overline{Z}}_b$ are hermitian symmetric, positive semidefinite matrices, (40) can be extremized as in the previous section to obtain the generalized eigenvalue problem

$$\overline{\overline{Z}}_a\, \overline{R} = \lambda\, \overline{\overline{Z}}_b\, \overline{R} \tag{42}$$

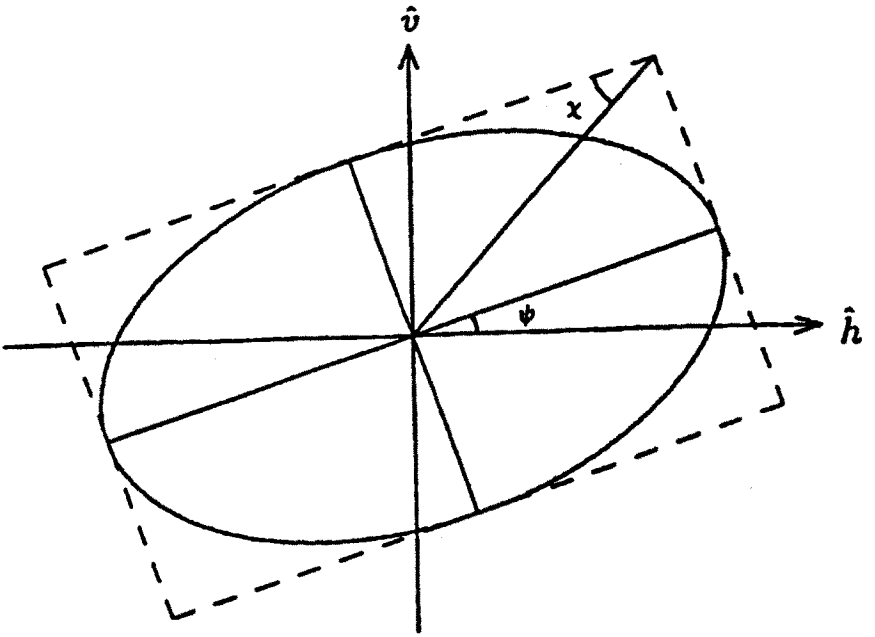

Figure 6.13 Generalized elliptic polarization state.

Once $\overline{R}$ is obtained, it should be normalized so that (22b) holds. Application of the transform given in (39) will yield $\overline{W}$.

d. Results and Discussion

In order to present the optimal polarimetric matched filtering results in a compact format, orientation (ψ) and ellipticity (χ) angles (Fig. 6.13) are utilized to express the transmitting and receiving polarization states. Here, the definitions from *Kong* [1986] are adopted. Therefore, horizontal (H) and vertical (V) polarization states will have zero degree ellipticity angles, with orientation angles of 0° and 90°. Right (R) and left (L) polarization states are orientation independent with ellipticity angles of 45° and −45°, respectively. In addition, $0° \leq \psi \leq 180°$ and $-45° \leq \chi \leq 45°$.

A general polarization vector,

$$\overline{P} = \begin{bmatrix} P_h \\ P_v \end{bmatrix} = \begin{bmatrix} |P_h| \exp(i\phi_h) \\ |P_v| \exp(i\phi_v) \end{bmatrix} \tag{43}$$

written in terms of horizontal ($\hat{h}$) and vertical ($\hat{v}$) vector components,

can be transformed into a normalized Stokes vector as follows

$$\begin{bmatrix} S_0 \\ S_1 \\ S_2 \\ S_3 \end{bmatrix} = \begin{bmatrix} |P_h|^2 + |P_v|^2 \\ |P_h|^2 - |P_v|^2 \\ 2|P_h||P_v|\cos\phi \\ 2|P_h||P_v|\sin\phi \end{bmatrix} = (|P_h|^2 + |P_v|^2) \begin{bmatrix} 1 \\ \cos 2\chi \cos 2\psi \\ \cos 2\chi \sin 2\psi \\ \sin 2\chi \end{bmatrix} \quad (44)$$

where $\phi = \phi_v - \phi_h$. Using this equation, the angles ψ and χ are obtained.

Two data bases were utilized to study the contrast problem, utilizing the techniques outlined in the previous sections. Table 6.4 gives polarimetric covariance statistics extracted from the San Francisco Bay area, L-band (1.225 GHz) SAR data, collected by the Jet Propulsion Laboratory's airborne polarimeter [*Zebker* et al., 1987]. These covariance statistics were obtained from the urban and park areas shown in Fig. 6.1 and were utilized to generate the results shown in Tables 6.7, 6.8, and 6.10. Similarly, the experimental polarimetric covariance data, shown in Table 6.5, were supplied by the MIT Lincoln Laboratory [*Borgeaud et al.*, 1987; *Kong et al.*, 1988]. This data, collected at 35 GHz, were used to generate the results presented in Table 6.9. The MIT Lincoln Laboratory radar imaged a vegetation field consisting of grass or trees at a range of approximately 2 kilometers. Studies using this database indicate that essentially no correlation exists between the HH and HV, and between the HV and VV polarimetric returns, i.e., the terrain clutter exhibits azimuthal symmetry.

	$\sigma(dB)$	e	γ	$\lvert\rho\rvert$	ϕ_ρ	$\lvert\beta\rvert$	ϕ_β	$\lvert\xi\rvert$	ϕ_ξ
Urban	-41.7	0.043	0.882	0.281	-179	0.640	-169	0.356	18.2
Park	-49.5	0.166	1.427	0.145	-21.8	0.082	-131	0.062	96.2

Table 6.4 Covariance matrix elements for park and urban (city) regions. Phase angles are given in degrees.

	$\sigma(dB)$	e	γ	$\lvert\rho\rvert$	ϕ_ρ
Trees	−13.0	0.06	1.1	0.74	0.0
Grass	−15.0	0.15	1.2	0.56	0.0

Table 6.5 Covariance matrix elements for a uniform terrain cover consisting of grass and tree regions.

Next, a comparison is made which evaluates the performance obtained by processing polarimetric radar data using the optimal polarimetric matched filter versus other commonly used polarization states. Linear weighting vectors which correspond to commonly used transmitting and receiving polarization states are given in Table 6.6. The weighting vectors presented in this table were generated using (23a) through (23c), (43) and (44). These linear weighting vectors are expressed in a horizontal-vertical polarization basis.

Table 6.7 presents theoretical contrast ratios r_{ab} and r_{ba} obtained when utilizing the above-mentioned transmitting and receiving polarization states (Table 6.6) as well as the optimal solution. Here, class A and B scatterers have been defined to denote the park and urban (city) regions, which were represented by their corresponding covariance matrices, $\overline{\overline{C}}_a$ and $\overline{\overline{C}}_b$, respectively. As previously discussed, for reciprocal backscattering the transmitting and receiving polarization state may be interchanged while maintaining the same contrast ratio. This is clearly indicated by the HV and VH results and the LR and RL results. The values r_{ab} and r_{ba}, which denote the maximum and reciprocal of the minimum eigenvalues found after solving (28), are expressed in terms of their corresponding orientation and ellipticity angles, ψ and χ. From Table 6.7 it is seen that the maximum contrast ratio between the two selected classes is 9.12 dB. Note that had only r_{ab} been maximized, a contrast ratio of 0.97 dB would have been realized. In some cases, though, this may be what is required. If the problem was only to make the park processed pixel intensity as large as possible with respect to that of the city, the transmitting and receiving polarization state corresponding to the average power ratio of 0.97 dB would be the appropriate matched filter which should be used to process data.

Table 6.8 shows the actual polarimetric contrast enhancement achieved when processing the radar measurements using the optimal polarimetric matched filter and various other polarization filters. Since the contrast ratios for r_{ba}, given in Table 6.7, are larger than those for r_{ab}, the linear weighting vectors which correspond to the contrast ratios for r_{ba} have been used to generate the results shown in Table 6.8. Thus, Table 6.8 contains the actual average processed pixel intensity realized for each of the two classes (urban and park areas) for both suboptimal polarization filters, i.e., transmitting and receiving polarization states which do not provide maximum contrast between classes, and

the optimal polarimetric matched filter. In comparing the data in this table, it is seen that the quantitative measure of attainable contrast is the contrast ratio, which is the linear ratio of (or the logarithmic *distance* between) the average pixel intensity for the two respective classes. In the case of processing data with the optimal polarimetric matched filter, this distance is maximum. Thus after optimal processing, it is possible to more readily separate the two classes than prior to it, since the distance between the average value of pixel intensity

Transmitting Polarization	Receiving Polarization	Linear Weighting Vector: $\overline{W}$
H	H	$\begin{bmatrix} 1.0 \\ 0.0 \\ 0.0 \end{bmatrix}$
H	V	$\begin{bmatrix} 0.0 \\ 1.0 \\ 0.0 \end{bmatrix}$
V	H	$\begin{bmatrix} 0.0 \\ 1.0 \\ 0.0 \end{bmatrix}$
V	V	$\begin{bmatrix} 0.0 \\ 0.0 \\ 1.0 \end{bmatrix}$
L	L	$\begin{bmatrix} 0.5 \\ i \\ -0.5 \end{bmatrix}$
L	R	$\begin{bmatrix} 0.5 \\ 0.0 \\ 0.5 \end{bmatrix}$
R	L	$\begin{bmatrix} 0.5 \\ 0.0 \\ 0.5 \end{bmatrix}$
R	R	$\begin{bmatrix} 0.5 \\ -i \\ -0.5 \end{bmatrix}$

Table 6.6 Commonly utilized transmitting and receiving polarization states versus their corresponding linear weighting vectors (expressed in a horizontal-vertical polarization basis).

Transmitting Polarization	Receiving Polarization	Contrast Ratio r_{ab} (dB)	Contrast Ratio r_{ba} (dB)
H	H	-7.86	7.86
H	V	-2.00	2.00
V	H	-2.00	2.00
V	V	-5.77	5.77
L	L	-7.62	7.62
L	R	-4.78	4.78
R	L	-4.78	4.78
R	R	-7.51	7.51
$\psi = 82.4$ $\chi = 2.25$	$\psi = 177.6$ $\chi = -2.43$	0.97	-0.97
$\psi = 23.5$ $\chi = -2.45$	$\psi = 129.5$ $\phi = 1.92$	-9.12	*9.12*

Table 6.7 Theoretical contrast ratios between classes when $\overline{\overline{C}}_a = Park$ and $\overline{\overline{C}}_b = Urban$ San Francisco Bay regions, respectively. Orientation and ellipticity angles are given in degrees. $\mathbf{MAX}_{\overline{W}}(r_{ab}) = 0.97$ dB, $\mathbf{MAX}_{\overline{W}}(r_{ba}) = 9.12$ dB, therefore $r = 9.12$ dB.

Transmitting Polarization	Receiving Polarization	Urban Class (dB)	Park Class (dB)	Contrast Ratio (dB)
H	H	-41.7	-49.5	7.8
H	V	-55.3	-57.3	2.0
V	V	-42.2	-48.0	5.8
L	L	-43.5	-51.2	7.7
L	R	-46.4	-51.2	4.8
R	R	-43.6	-51.1	7.5
$\psi = 23.5$ $\chi = -2.45$	$\psi = 129.5$ $\chi = 1.92$	-43.8	-52.9	*9.1*

Table 6.8 Actual average pixel intensities and the contrast ratios between the park and urban San Francisco Bay regions when data were processed using commonly employed polarization filters and the optimal polarimetric matched filter.

Transmitting Polarization	Receiving Polarization	Contrast Ratio r_{ab} (dB)	Contrast Ratio r_{ba} (dB)
H	H	2.00	−2.00
H	V	−1.98	1.98
V	H	−1.98	1.98
V	V	1.62	−1.62
L	L	−1.00	1.00
L	R	2.28	−2.28
R	L	2.28	−2.28
R	R	−1.00	1.00
$\psi = 0$ $\chi = 0$	$\psi = 90$ $\chi = 0$	−1.98	1.98
$\psi \simeq 0$ $\chi = -38.3$	$\psi \simeq 0$ $\chi = 38.3$	*2.31*	−2.31

Table 6.9 Theoretical contrast ratios between classes when trees = a and grass = b for class A and B scatterers, respectively. Orientation and ellipticity angles are given in degrees. $\mathbf{MAX}_{\overline{W}}(r_{ab}) = 2.30$ dB, $\mathbf{MAX}_{\overline{W}}(r_{ba}) = 1.99$ dB, therefore $r = 2.30$ dB.

Transmitting Polarization	Receiving Polarization	Contrast Ratio (dB)
H	$\psi = 142.1$ $\chi = 0.51$	8.21
V	$\psi = 44.8$ $\chi = 0.75$	6.10
R	$\psi = 27.5$ $\chi = 23.1$	7.87
L	$\psi = 169.6$ $\chi = -23.6$	7.98
$\psi = 23.5$ $\chi = -2.45$	$\psi = 129.5$ $\chi = 1.92$	*9.12*

Table 6.10 Optimal receiving polarization state for a fixed transmitting polarization state when $\overline{\overline{C}}_a = Park$ and $\overline{\overline{C}}_b = Urban$ San Francisco Bay regions. Orientation and ellipticity angles are given in degrees.

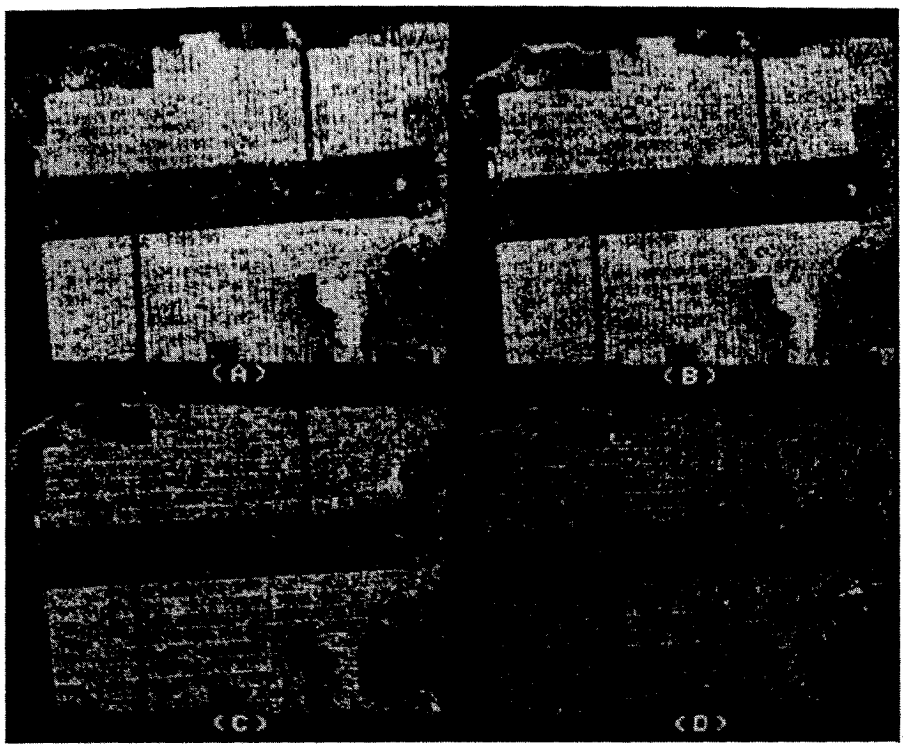

Figure 6.14 San Francisco Bay area images synthesized using the optimal polarimetric matched filter (A), HH (B), VV (C), and HV (D) polarization filters. The corresponding contrast ratios between the city and park region were 9.1, 7.8, 5.8, and 2.0 dB, respectively.

has increased between the two classes. Also note that the contrast ratios, shown in Table 6.8, and those given in Table 6.7 for r_{ba}, are similar indicating a good match between the theoretical predictions and the processed results.

A further demonstration of contrast enhancement can be seen visually by comparing Figs. 6.14A through 6.14D which show San Francisco Bay area images. This imagery has been synthesized utilizing some commonly employed linear polarization states, in addition to the transmitting and receiving polarization state required to produce maximum contrast between the park and urban regions. In all four of these

images, the average processed pixel intensity of the park region was set to the baseline value, i.e, the minimum quantization level of the imaging system display, which was −20 dB. The maximum quantized intensity was −10 dB. By utilizing these quantization limits, some clipping of the higher and lower intensity levels has occurred. This procedure was implemented to compare more easily the contrast between images. Figure 6.14A illustrates the result of processing the San Francisco Bay polarimetry using the optimal polarimetric matched filter. The contrast ratio obtained between the city and park area, as previously indicated in Table 6.8, was 9.1 dB. Contrast ratios achieved using HH (Fig. 6.14B), VV (Fig. 6.14C), and HV (Fig. 6.14D) polarization filters were only 7.8, 5.8, and 2.0 dB, respectively. As indicated in Table 6.8, utilizing the optimal transmitting and receiving polarization state, i.e., the optimal polarimetric matched filter, to process data yields the maximum contrast ratio. Figure 6.14 also shows that the optimal and HH synthesized images appear somewhat similar; this is due to the fact that there is only a 1.2 dB difference between their contrast ratios. However, the optimal polarimetric matched filter always yields a larger contrast ratio between classes than when any other transmitting and receiving polarization states are utilized.

Contrast ratio results, obtained using the MIT Lincoln Laboratory data are presented in Table 6.9. As was the case in Table 6.7, theoretical contrast ratios are given for frequently employed polarization states as well as for the optimal solution. In this table, the tree and grass regions have been arbitrarily selected to denote class a and b scatterers, respectively. The optimal solution again is represented by its corresponding orientation and ellipticity angles ψ and χ, in which case the values presented for r_{ab} and r_{ba}, shown in Table 6.9, signify the maximum and reciprocal of the minimum eigenvalues found when employing the equations shown in (36a) and (36b).

In Table 6.10, the optimal receiving polarization states required to produce the maximum contrast ratio between classes for various fixed transmitting polarization states are presented. These results show that by employing the optimal receiving polarization state, all contrast ratios have increased relative to those shown in Table 6.7 or 6.8. Thus, for a given transmitting polarization state, synthesizing imagery using the optimal receiving polarization state always yields a larger contrast ratio than when any other polarization state is used. However, the

maximum contrast ratio is achieved only when the optimal transmitting and receiving polarization state is employed.

Acknowledgments

This work was supported by NASA Contract 958461, NASA Contract NAGW-1617, NASA Contract NAGW-1272, ARMY Corp of Engineers Contract DACA39-87-K-0022, and ONR Contract N00014-89-J-1107. The authors would like to thank the Jet Propulsion Laboratory Radar Program for supplying the experimental data presented in this chapter.

References

[1] Borgeaud, M., R. T. Shin, and J. A. Kong, "Theoretical models for polarimetric radar clutter," *J. Electromag. Waves Appl.*, **1**, **1**, 67–86, 1987.

[2] Cadzow, J. A., "Generalized digital matched filtering," Proc. 12, Southeastern Symposium on System Theory, Virginia Beach, VA., 307–312, May 1980.

[3] Ecker, H. A., and J. W. Cofer, Jr., "Statistical characteristics of the polarization power ratio for radar return with circular polarization," *IEEE Trans. Aero. Electro. Sys.*, **AES-5**, **5**, 762–769, 1969.

[4] Evans, D. L., T. G. Farr, J. P. Ford, T. W. Thompson, and C. L. Werner, "Multipolarization radar images for geologic mapping and vegetation discrimination," *IEEE Trans. Geosci. Remote Sens.*, **GE-24**, **2**, 246–256, 1986.

[5] Fukunaga, K., *Introduction to Statistical Pattern Recognition*, Academic Press, New York, 51–55, 1972.

[6] Giuli, D., M. Gherardelli, and E. Dalle Mese, "Performance evaluation of some adaptive polarization techniques," *Proc. IEEE Intl. Radar Conference*, 76–81, London, U.K., Oct. 1982.

[7] Giuli, D., "Polarization diversity in Radars," *Proc. IEEE*, **74**, **2**, 245–269, Feb. 1985.

[8] Huang, T. S., "Image enhancement: A review," *Opto-Electronics,* **1,** 49–59, 1969.

[9] Huynen, J. R., "Phenomenological theory of radar targets," Edited by Piergirogio L. E. Uslenghi, *Electromagnetic Scattering,* Academic Press, New York, 653–712, 1978.

[10] Ioannidis, G. A., and D. E. Hammers, "Optimum antenna polarization for target discrimination in clutter," *IEEE Trans. Ant. Prop.,* **AP-27, 3,** 357–363, May 1979.

[11] Kong, J. A., A. A. Swartz, H. A. Yueh, L. M. Novak, and R. T. Shin, "Identification of terrain cover using the optimum polarimetric classifier," *J. Electromag. Waves Appl.,* **2, 2,** 171–194, 1988.

[12] Kong, J. A., *Electromagnetic Wave Theory,* John Wiley & Sons, New York, 16–24, 1986.

[13] Kostinski, A. B., and W. M. Boerner, "On the polarimetric contrast optimization," *IEEE Trans. Ant. Prop.,* **AP-35, 8,** 988–991, August 1987.

[14] Kozlov, A. I., "Radar contrast between two objects," *Radioelectronika,* **22, 7,** 63–67, July 1979.

[15] Kriegler, F. J., W. A. Malila, R. F. Nalepka, and W. Richardson, "Preprocessing transformations and their effects on multispectral recognition," *Proc. Sixth International Symposium on Remote Sensing of Environment,* **1,** Environmental Research Institute of Michigan, Ann Arbor, Mich., 97–131, 1971.

[16] Lim, H. H., A. A. Swartz, H. A. Yueh, J. A. Kong, R. T. Shin, and J. J. van Zyl, "Classification of earth terrain using polarimetric synthetic aperture radar images," *J. Geophys. Res.,* **94, B6,** 7049–7057, 1989.

[17] McCormick, G. C., and A. Hendry, "Optimal polarizations for partially polarized backscatter," *IEEE Trans. Ant. Prop.,* **AP-33, 1,** 33–39, Jan. 1985.

[18] Mieras, H., "Optimal polarizations of simple compound targets," *IEEE Trans. Ant. Prop.,* **AP-31, 6,** 996–999, Nov. 1983.

[19] Nespor, J. D., A. P. Argawal, and W. M. Boerner, "Development of a model-free clutter description based on a coherency matrix

formulation," *IEEE Ant. Prop. Society*, International Symposium Digest, 37–40, 1984.

[20] Rice, S. O., "Reflection of electromagnetic waves from slightly rough surfaces," *Commun. Pure Appl. Math.*, **4**, 351–378, 1951.

[21] Richards, J. A., G. Sun, and D. Simonett, "L-band radar backscatter modeling of forest stands," *IEEE Trans. Geosci. Remote Sens.*, **GE-25**, 487–498, 1987.

[22] Smedes, H. W., M. M. Spencer, and F. J. Thomson, "Preprocessing of multispectral data and simulation of ERTS data channels to make computer terrain maps of a Yellowstone National Park test site," *Proc. Seventh International Symposium on Remote Sensing of Environment*, **3**, Ann Arbor, Michigan, 2073–2094, 1971.

[23] Swartz, A. A., H. A. Yueh, J. A. Kong, L. M. Novak, and R. T. Shin, "Optimal polarizations for achieving maximum contrast in radar images," *J. Geophys. Res.*, **93, B12**, 15252–15260, 1988.

[24] Urkowitz, H., *Signal Theory and Random Processes*, Artech House, Inc., 293, 1983.

[25] van Zyl, J. J., C. H. Papas, and C. Elachi, "On the optimal polarizations of incoherently reflected waves," *IEEE Trans. Ant. Prop.*, **AP-35, 7**, 818–826, July 1987.

[26] van Zyl, J. J., H. A. Zebker, and C. Elachi, "Imaging radar polarization signature: Theory and observation," *Radio Science*, **22, 4**, 529–543, July–Aug., 1987.

[27] van Zyl, J. J., "Unsupervised classification of scattering behavior using radar polarimetry data" *IEEE Trans. Geosci. Remote Sens.*, **GE-27, 1**, 36–45, 1989.

[28] Wu, S. T., and S. A. Sader, "Multipolarization SAR data for surface feature delineation and forest vegetation characterization," *IEEE Trans. Geosci. Remote Sens.*, **GE-25, 1**, 67–76, 1987.

[29] Yueh, H. A., A. A. Swartz, J. A. Kong, R. T. Shin, and L. M. Novak, "Optimal classification of terrain cover using normalized polarimetric data," *J. Geophys. Res.*, **93, B12**, 15261–15267, 1988.

[30] Zebker, H. A., J. J. van Zyl, and D. N. Held, "Imaging radar polarimetry from wave synthesis," *J. Geophys. Res.*, **92, B1**, 683–701, 1987.

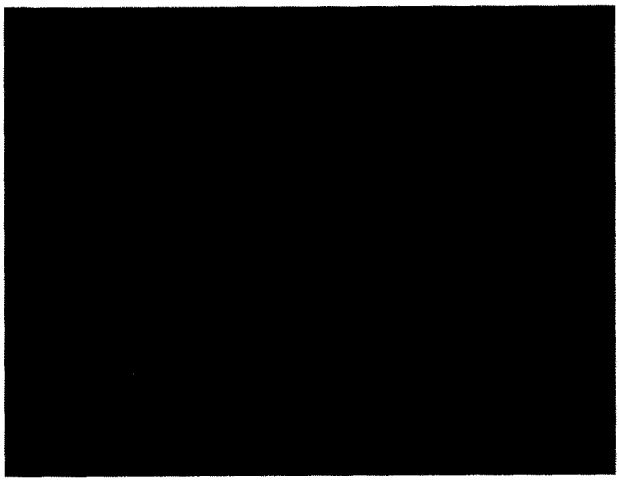

Plate 6.1

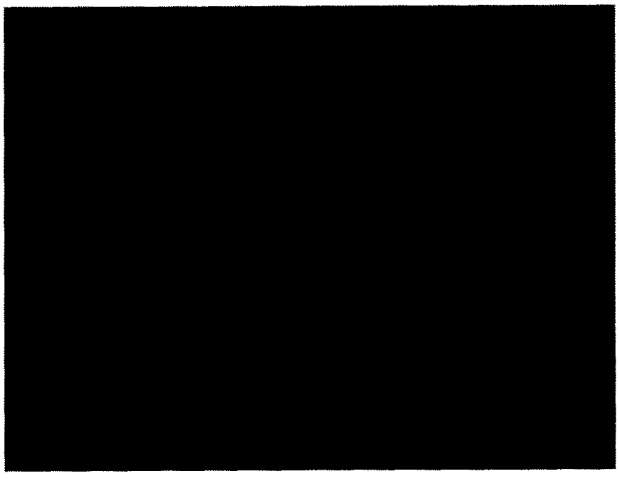

Plate 6.2

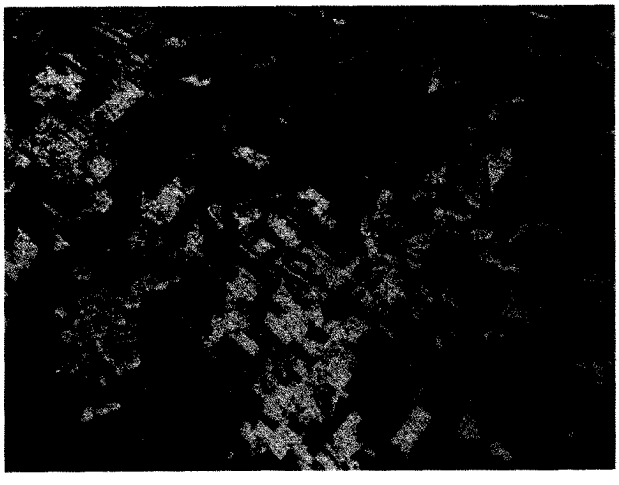

Plate 6.3

Plate 6.4

Plate 6.5

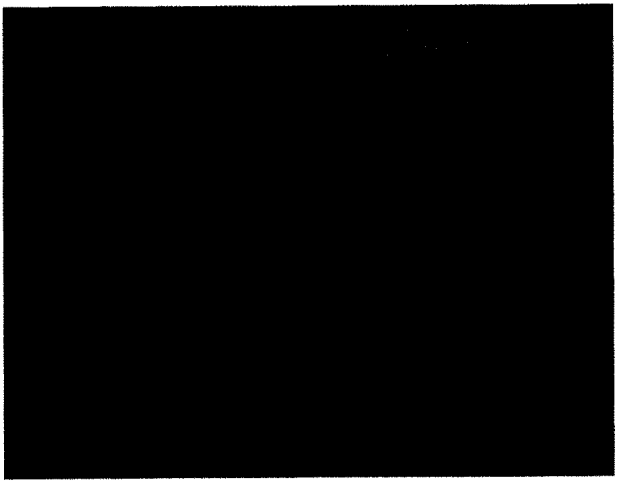

Plate 6.6

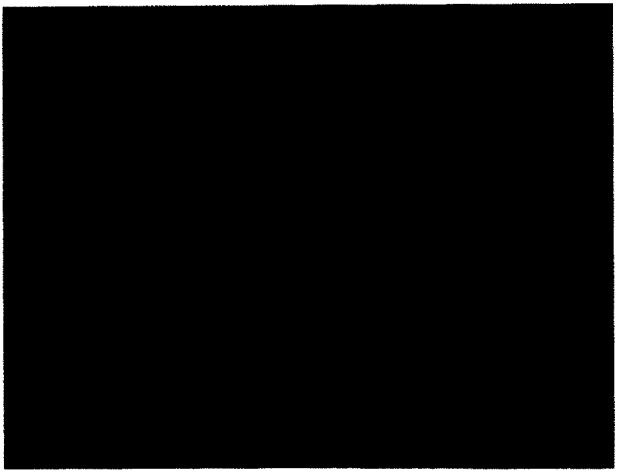

Plate 6.7

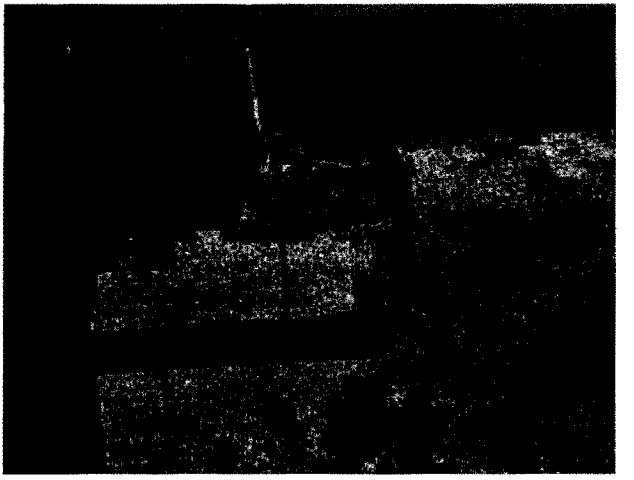

Plate 6.8

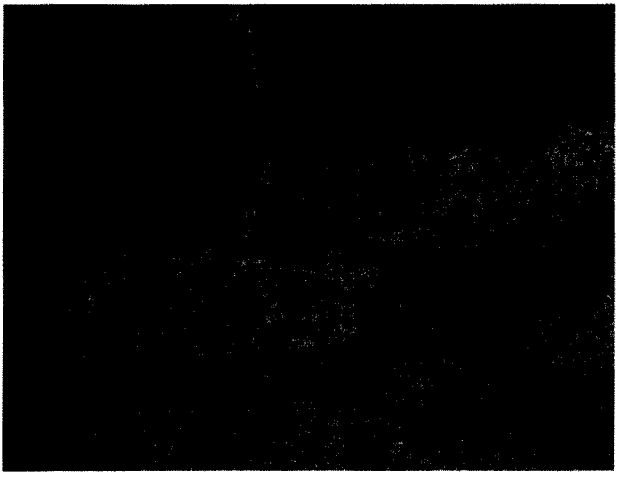

Plate 6.9

Plate 6.10

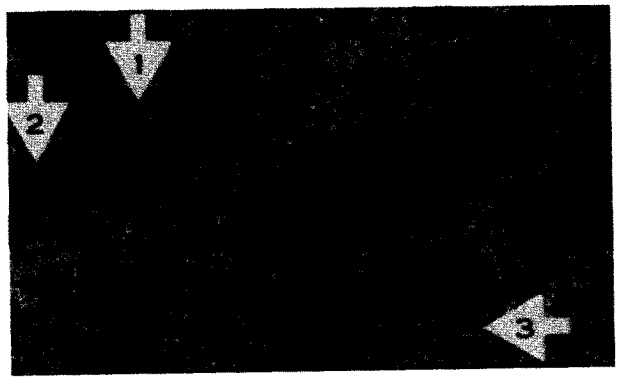

Plate 7.1

(a)

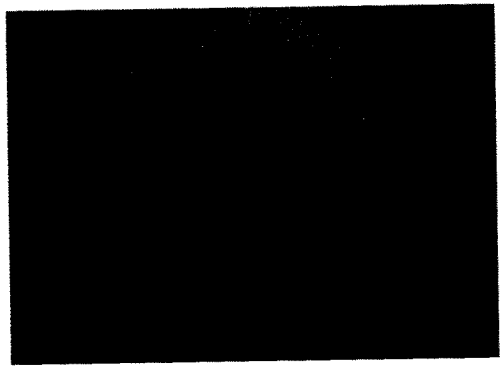

(b)

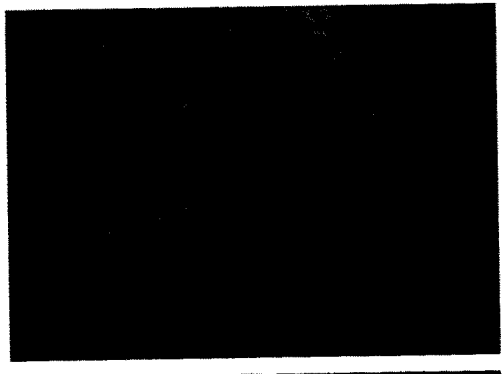

(c)